SHIPS AND OFFSHORE STRUCTURES
https://doi.org/10.1080/17445302.2021.1907071

Taylor & Francis
Taylor & Francis Group

OPEN ACCESS Check for updates

Prediction of cavitating propeller underwater radiated noise using RANS & DES-based hybrid method

Savas Sezen, Mehmet Atlar and Patrick Fitzsimmons

Department of Naval Architecture Ocean, & Marine Engineering, University of Strathclyde, Glasgow, UK

ABSTRACT

This study focuses on the prediction of the hydrodynamic and hydroacoustic performance of a cavitating marine propeller in open water condition using Reynolds-averaged Navier-Stokes (RANS) and Detached Eddy Simulation (DES) solvers. The effectiveness of the methods is investigated for the recently introduced benchmark propeller that belongs to the research vessel 'The Princess Royal'. The main emphasis of the study is to examine the capabilities of the RANS and DES solvers for predicting the hydrodynamic performance of a propeller in the presence of sheet and tip vortex cavitation (TVC). In the numerical simulations of the cavitating propeller flow, the Schnerr-Sauer cavitation model based on a reduced Rayleigh-Plesset equation was used to model the sheet and tip vortex cavitation. An alternative Vorticity-based Adaptive Mesh Refinement (V-AMR) technique was employed for the accurate realisation of the TVC in the propeller's slipstream. In the hydroacoustic calculations, a porous Ffowcs Williams Hawkings equation (P-FWH) was employed together with the DES solver. The numerical hydrodynamic and hydroacoustic results are compared with those of experimental data for the benchmark propeller available from the University of Genova Cavitation Tunnel. The results show that both the RANS and DES solvers are successful for modelling of the sheet cavitation on the propeller blades. However, the prediction of the TVC extension using the RANS solver is found to be insufficient in comparison to the TVC prediction when using the DES method. This is due to the inherent modelling limitations of the RANS solver. In addition to hydrodynamic performance predictions, the overall noise spectrums were found in an agreement with the experimental data with discrepancies between the low and high-frequency region.

ARTICLE HISTORY
Received 31 October 2020
Accepted 4 March 2021

KEYWORDS
RANS; DES; Tip Vortex Cavitation; FWH; Underwater Noise; The Princess Royal

1. Introduction

Ambient noise levels of the world's oceans have surged due to the rapid increase of anthropogenic and natural sources. Amongst different type of noise sources, the noise induced by the shipping activities mainly dominates the low-frequency range of the noise spectrum. Since this range is also crucial for the survivability of the marine animals, a more accurate prediction and mitigation of the underwater radiated noise (URN) has become a great interest in recent years (Urick 1983; Hildebrand 2009). Thus, international associations, classification societies and conservation groups have recognised this issue and advised the industry to take the precautions to mitigate its harmful effects on marine fauna (Kellett et al. 2013). Moreover, the International Maritime Organization (IMO) has published a non-mandatory guideline for commercial ships to give general advice for the mitigation of the noise levels (IMO 2014).

As far as shipping noise is concerned, a ship can experience different noise sources such as machinery & auxiliary engine noise, flow-induced noise, and non-cavitating and cavitating propeller radiated noise. Amongst these sources, the cavitating propeller is the most dominant one contributing to the overall radiated noise levels. Due to this fact, the prediction of the propeller cavitation noise has been a great interest for the military and commercial purposes for years (Tani et al. 2019a). From the military point of view, the propeller URN characteristics of the naval vessels (e.g. submarines) is also critical for their design because of the crucial requirements for the stealth mode of operations and acoustic detection.

In order to predict the propeller URN under non-cavitating and cavitating conditions, model tests conducted in cavitation tunnels & depressurised tanks and some semi-empirical methods have been utilised. Some research programmes and campaigns were also undertaken, relatively recent, to have a better understanding of the URN and complex flow phenomena (e.g. including cavitation dynamics) using experimental techniques. In the scope of European R&D projects (e.g. SILENV ; AQUO ; SONIC) under the 7th Framework Programme (FP) of the EU, the URN induced by the commercial shipping was investigated with the contributions of several hydrodynamic institutes, noise experts, shipyards, universities, etc. Additionally, as there is no universal procedure for the measurement of a URN, this required investigations on the accuracy and reliability of the URN measurement techniques at model as well as in full-scale. Therefore, the test procedures, which are implemented in the tunnels or depressurised tanks, were explored by using the same benchmark model propeller in the scope of a round-robin (RR) test campaign by the contribution of various facilities and universities (Tani et al. 2019b). Within this framework, joint research programme

CONTACT Savas Sezen savas.sezen@strath.ac.uk

© 2021 The Author(s). Published by Informa UK Limited, trading as Taylor & Francis Group
This is an Open Access article distributed under the terms of the Creative Commons Attribution-NonCommercial-NoDerivatives License (http://creativecommons.org/licenses/by-nc-nd/4.0/), which permits non-commercial re-use, distribution, and reproduction in any medium, provided the original work is properly cited, and is not altered, transformed, or built upon in any way.

(JRP), named 'Noise Measurements', was conducted with the Hydro Testing Alliance Network of Excellence (HTA-NoE). The programme completed its mission successfully in 2011 (AMT'11 2011). However, the URN investigations under the activities of a new working group, which is known as Noise Community of Practice (Noise CoP) of the Hydro Testing Forum (HTF), were carried on with the members of HTA-NoE. Thus, a round-robin (RR) test programme was organised to predict the cavitation and URN for the Newcastle University's (UNEW) Deep-V type catamaran research vessel *The Princess Royal* (Atlar et al. 2013). The Noise CoP aimed to develop and present the URN measurement techniques including cavitation modelling and noise predictions with the contributions of different facilities (e.g. the University of Genoa UNIGE, University of Strathclyde, NMRI, SSPA, KRISO, CNR-INM, and MARIN) for the Princess Royal's propeller in model scale. The first experimental results of the Princess Royal propeller were presented in the study of Tani et al. (2019b). In this study, the experimental setups and data analysis methods of the different facilities, including the cavitation observations and noise characteristics of the propeller, were presented under the uniform flow conditions.

On the other hand, as well as the noise measurements in the cavitation tunnels or depressurised tanks, Computational Fluid Dynamics (CFD) methods have become popular for the solution of complex flow (e.g. cavitation) around the propeller with the development of the computational tools (e.g. Bensow and Bark 2010; Tani et al. 2019a). To this aim, benchmark propellers (e.g. Potsdam Propeller Test Case (PPTC), INSEAN E779A) were used for the validation of different numerical techniques, which were applied by different facilities, with the experimental cavitation observations and hydrodynamic results (Salvatore et al. 2009; SMP11 2011). In the numerical calculations, the flow around the cavitating marine propeller is deemed to be more complicated than the non-cavitating case. The reason being, there is a strong interaction between the cavitation dynamics and turbulence (Bensow and Bark 2010; Usta and Korkut 2018). In the past, the studies of the propeller cavitation have commonly focused on the prediction of sheet cavitation using viscous and potential solvers (e.g. Kinnas and Fine 1992; Bal 2011; Sipilä 2012). However, one of the challenging phenomena is to model the TVC for marine propellers. TVC generally occurs as the first type of cavitation on well-designed propellers, and it is one of the important sources of a URN, especially in the presence of the bubble collapse or bursting phenomenon which commonly occurs in the non-uniform wake. Thus, its avoidance or delay has a great interest in naval, cruise and research vessels which need to radiate low URN (Gaggero et al. 2014).

In order to understand the dynamics of the tip vortex, the non-cavitating tip vortex flows have still been explored using viscous solvers (i.e. RANS, DES and Large Eddy Simulation (LES)) in the literature (e.g. Muscari et al. 2013; Peng et al. 2013; Guilmineau et al. 2015). The numerical studies showed that RANS solvers could be reliably used as a design tool for the cavitating flows, particularly in the presence of sheet cavitation. However, RANS solvers have been generally discussed in terms of accurate assessment of the tip vortex flows in the literature. Hence, more advanced numerical models (i.e. DES and LES) are alternative ways for a more realistic modelling of the tip vortex flow. As well as the non-cavitating tip vortex-related studies, the behaviour and modelling of the cavitating tip vortex have also been widely investigated (e.g. Gaggero et al. 2014; Sipilä et al. 2014; Viitanen and Siikonen 2017). As a result of the several numerical investigations based on CFD methods, it has become clear that the accurate prediction and observation of the TVC mainly depend on both adequate cell size inside the vortex region and turbulence modelling. Thus, a priory local mesh refinement is widely used for the observation of TVC for the isolated propeller and complete ship model (i.e. hull together with propeller). However, these approaches are still not completely successful and increase the computational cost of the solution considerably due to the rapid increase in the total element count. Moreover, it is also not possible to adopt the high-resolution grids in the entire propeller's slipstream as it would also increase the computational time & cost excessively. Therefore, it is necessary to refine the grid as locally as possible for the solution of TVC using AMR technique. In this way, the computational time & cost of numerical solutions can be significantly reduced. Within this perspective, the current study presents an alternative vorticity-based AMR (V-AMR) technique to improve the capturing of TVC in the propeller's slipstream.

Not only are potential and viscous solvers being used to predict hydrodynamic performance (e.g. thrust and torque), but they are now being combined/coupled with acoustic analogies for the prediction of propeller URN. In this way, the hydrodynamic and hydroacoustic fields are decoupled; thus, the required input data for acoustic analogy is provided with the hydrodynamic solver. This procedure is also known as a hybrid method (i.e. hydrodynamic solver with the acoustic analogy). The most commonly used acoustic analogy is the Ffowcs-Williams Hawkings (FWH) equation in both aeroacoustics and hydroacoustic fields. In the aeroacoustics field, the impermeable formulation of FWH equation has been generally used for the noise prediction by taking only linear terms (i.e. monopole and dipole noise terms) into account. The reason being that the flow regime is often assumed as subsonic due to the low rotational speed of the blades. The non-linear term (i.e. quadrupole noise term) in the aero-acoustic field becomes important at high supersonic or transonic regimes. However, in the presence of cavitation, the non-linear and turbulent vortex structures in the propeller's wake can also give a significant contribution to the overall noise levels even if the cavitation is more dominant. Thus, the non-linear term of the FWH equation needs to be included in the calculations, either solving the direct volume integrals or using the porous FWH (P-FWH) formulation. However, the solution of direct volume integrals is computationally expensive and more sensitive to the accuracy of the input data in original formulation. Due to this reason, P-FWH equation becomes attractive as the quadrupole volume integrals are evaluated with the solution of surface integrals. The application of the FWH acoustic analogy with the hydrodynamic solver is a relatively new research area to predict the URN for maritime problems. Early investigations in the open literature were concentrated on the non-cavitating propeller URN to understand the mechanism of the URN and sensitivity of the FWH acoustic analogy

(e.g. Ianniello et al. 2013; LLoyd et al. 2015; Testa et al. 2018; Sezen and Kinaci 2019). Nowadays, the investigations have been focusing on the cavitating URN studies using advanced numerical techniques and FWH acoustic analogy (e.g. Bensow and Liefvendahl 2016; Lidtke et al. 2019). Within this framework, the present authors also presented some preliminary results of the cavitating URN for the Princess Royal propeller in the low-frequency region of the noise spectrum using RANS solver replicating the free-field condition (Sezen et al. 2019; Sezen et al. 2020). The detailed investigation of the preliminary results showed that the cavitation pattern on the propeller blades was generally overpredicted. However, some part of the overprediction was associated with a detailed description of the blade geometry.

Despite increasing numbers of recent studies for the better modelling and simulations of TVC using CFD solvers, the details and effectiveness of these solvers have not been completely understood. Also, to the best of the authors' knowledge, there exists no specific numerical study to predict the propeller URN in cavitating condition including the TVC by using an advanced hybrid model (i.e. DES with P-FWH equation) for a realistic test configuration. Thus, the present study aims to fill this research gap in the literature by exploring the pros and cons of RANS and DES solvers with newly proposed V-AMR technique in a commercial CFD solver for the better TVC modelling and hence resulting URN predictions.

Within the framework of the above aim, the numerical models used in this study are presented in Section 2 of the paper. The overview of the test case setup for the benchmark propeller in open water condition is given in Section 3. The computational domain, boundary conditions and grid structure, including the AMR implementation, are presented in Section 4. The numerical results are presented and discussed in Section 5. Finally, conclusions and recommendations for future work are given in Section 6.

2. Theoretical and numerical models

2.1. Hydrodynamic model

The simulations for the benchmark propeller flow in the open water condition were conducted using the commercial CFD solver, Star CCM+, including cavitation modelling (Star CCM 14.06+ 2019) The flow solver uses a finite volume method to discretise the governing equations for the numerical modelling of the flow field around the propeller.

In the numerical calculations, the k-ω SST turbulence model was used both for the RANS and Delayed-Detached Eddy Simulation (DDES) solvers. DES is a hybrid method that combines of RANS in the boundary layer and LES in the free field region. Although the RANS solvers are generally conducted for engineering purposes and used in the initial design stage, the scale resolving simulations (e.g. DES or LES) are preferred for more in-depth studies to solve the turbulent scales and cavitation dynamics accurately. Therefore, DES solver is an alternative way to decrease the computational cost of the LES approach, which needs high-resolution grids in all directions. Additionally, the application of DES solvers enables a realistic solution of the hydrodynamic flow field, which is not possible using the RANS solvers (Spalart et al. 2006; Star CCM 14.06+ 2019).

From the hydroacoustic perspective, RANS methods can be generally used to determine the blade harmonics in the low-frequency region. However, RANS methods are not suitable to predict the broadband noise, which is mainly dominated by turbulence and complex cavitation dynamics. The reason behind this is that RANS solvers take the average of the flow field for modelling the turbulent scales. Due to the higher computational cost of the LES solver, the hybrid RANS-LES method (i.e. DES) offers an alternative approach to capture the hydrodynamic sources of the noise by utilising the P-FWH approach (ITTC 2017).

The segregated flow model was used in the present numerical solver. The second-order scheme, which is suitable and advisable, especially for the DES method, was used for the convection term. The qualitative idea about the level of DES solution can be seen in Figure 1. F_{DES} is the DES Correction Factor and it shows the regions in the computational domain where the RANS and LES solvers are implemented in the DES solver. The correction factor calculation is based on the modification of the dissipation term in the transport equation. According to this correction factor, the $F_{DES} = 1$ shows the region where the unsteady RANS solution is provided, whereas $F_{DES} > 1$ shows the region where the LES solver is used. As can be clearly seen, the resolution of the propeller slipstream was provided by the LES approach in the DES solver.

The second-order implicit unsteady scheme was employed for time discretisation for both RANS and DES solvers. The

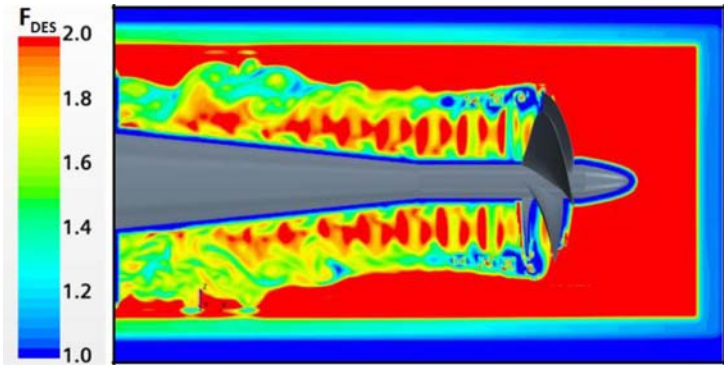

Figure 1. Visualisation of DES Correction Factor (RANS is $F_{DES} = 1$ and LES is $F_{DES} > 1$). (This figure is available in colour online.)

timestep is one of the vital parameters which is linked to Courant–Friedrichs–Lewy (CFL) number in the fluid domain. Particularly, for DES simulations, it was aimed to have CFL condition below 1, especially in the areas of interest provided by LES (e.g. propeller slipstream). Although CFL requirement is not related to the stability of the time scheme as the numerical approach is implicit, it is crucial to keep in the desired range for the accuracy of the solution (Star CCM 14.06+ 2019). Having said that the time step should be selected between 0.5 and 2 degrees of the propeller's rotational rate according to the International Towing Tank Conference guideline (ITTC 2011). Hence, the time step was selected as 0.5 degree of the propeller's rotational rate (i.e. around 3.968×10^{-5} s) to satisfy the CFL condition in the propeller's slipstream for both methods. The y^+ value is a non-dimensional number and it is used to distinguish the regions near the wall (i.e. in the boundary layer). The y^+ is calculated using the following equation (Wilcox 2006).

$$y^+ = \frac{U^* \Delta x}{\nu} \tag{1}$$

where U^* is the frictional velocity at the first cell near the wall (m/s), Δx is the distance between the wall and the first cell near the wall (m), ν is the kinematic viscosity of the fluid (m^2/s). The average wall y^+ value for the propeller blades was calculated to be around 0.7 for both RANS and DES simulations since the same grid structure was adopted. In this way, the boundary layer of the flow was resolved instead of using wall functions to increase the accuracy of the solution.

The simulations were initialised with the steady approach using Moving Reference Frame (MRF) for non-cavitating conditions and then switched to unsteady with the Rigid Body Motion (RBM), which is also known as the sliding mesh technique. The Volume of Fluid Approach (VOF) with Schnerr-Sauer cavitation model was employed to model the phase change. The VOF method was used to describe the phase transition of liquid into vapour or vice versa. The customisable cavitation parameters such as seed diameter and density are available in the facilities of Star CCM 14.06+ 2019. The influence of change in seed density and diameter on sheet and tip vortex cavitation was comprehensively investigated and the default values' accuracy was proved for the model scale propeller. Therefore, in the current study, the defaults values were used for the seed density 10^{12} ($1/m^3$) and seed diameter 10^{-6} m in the cavitation modelling (Star CCM 14.06+ 2019). The detailed information about cavitation modelling can be found in Schnerr and Sauer (2001). Once the flow field converged and the AMR procedure was applied, the acoustic pressures were collected during six propeller revolutions.

2.2. Hydro-acoustic model

The potential and viscous based solvers are firstly applied for the solution of the flow field around the marine propellers. In this way, the source field is identified using the incompressible solver, while the acoustic analogy is further used to transfer the information from near field to far-field as a transfer function. The Ffowcs Williams-Hawkings acoustic analogy (Williams and Hawkings 1969), which is the rearranged form of the continuity and momentum equations into the inhomogeneous wave equation, was used to predict the propeller URN in this study. FWH equation is an extended version of Lighthill's equation (Lighthill 1952) to predict the noise induced by arbitrary bodies. The source terms are identified at the right-hand side of the FWH formulation for the sound propagation (e.g. see Equation (2)).

The total acoustic pressure with respect to a receiver position and time can be given as in Equation (2), where the pressure is divided into three different parts by utilising the green functions.

$$p = p_T(x, t) + p_L(x, t) + p_Q(x, t) \tag{2}$$

where x and t are the receiver position and time, respectively. p is the total acoustic pressure (Pa), p_T is the thickness noise term (or monopole), p_L is the loading noise term (or dipole) and p_Q is the quadrupole (or non-linear) term. The first two terms are evaluated by solving the surface integral, whereas the latter one is evaluated by solving the volume integral. In the P-FWH approach, the physical meaning of the thickness and loading noise term loses its importance and the new terms appear as pseudo-thickness and pseudo-loading. In the P-FWH equation, the quadrupole noise sources are evaluated with the solution of surface integrals. In the current approach, it is assumed that the integral surface includes all relevant non-linear noise contribution as much as needed; hence, the non-linear contribution outside the integral surface was ignored.

In the presence of a porous version of the FWH equation, which was applied in (Williams and Hawkings 1969) but it was proposed as a possible solution of the FWH equation by and implemented in (Di Francescantonio 1997), two new variables were introduced as modified velocity and stress tensor. For a stationary domain and incompressibility, the porous formulation of FWH can be written as follows

$$4\pi p(x, t) = \int_S \frac{\rho_0 \dot{U}_n}{r} dS + \int_S \frac{\dot{L}_r}{c_0 r} dS + \int_S \frac{L_r}{r^2} dS + p_Q(x, t) \tag{3}$$

where r (m) is the distance between the noise source and the receiver, subscripts r and n define the dot product of a quantity with a unit vector either in radiation (radial) or normal directions, respectively. U and L are the modified velocity and stress tensor, respectively.

3. Test case set-up

The Princess Royal propeller was selected as a benchmark propeller for the investigation of hydrodynamic and hydroacoustic performance in the scope of this study. Apart from experimental results in model scale, the full-scale results in the presence of hull are available from the sea-trial data, which is the main focus of the ongoing studies. Figure 2 and Table 1 show the general view of the propeller and its main particulars, respectively.

In the scope of the round-robin (RR) test campaign, the benchmark propeller URN was predicted in several conditions (e.g. uniform and inclined) by different facilities. In this study, uniform flow condition was simulated, and results were

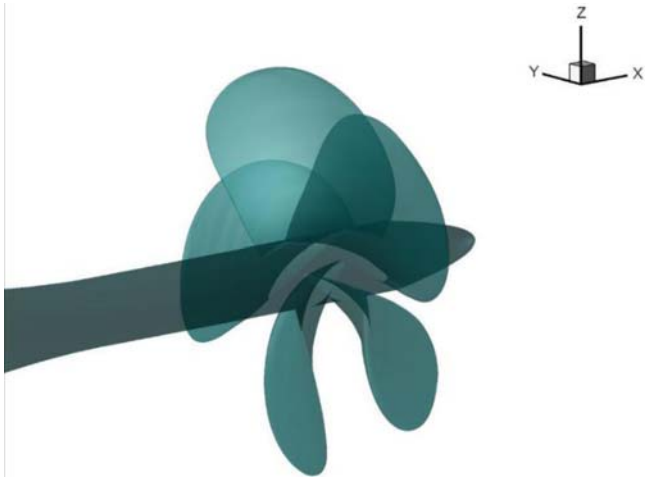

Figure 2. General view of the Princes Royal propeller. (This figure is available in colour online.)

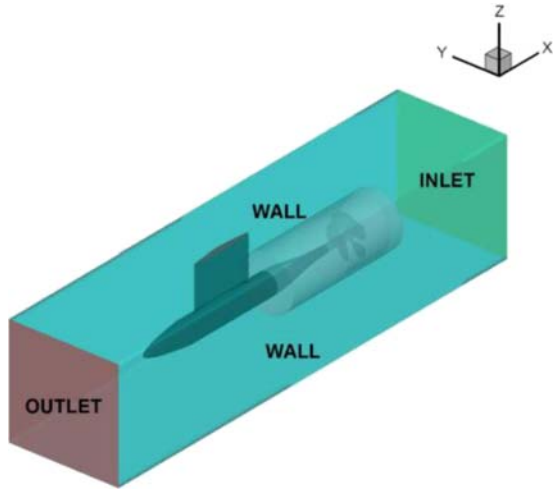

Figure 3. Computational domain for Princess Royal Propeller. (This figure is available in colour online.)

Table 1. The main particulars of the propeller.

Propeller Diameter (m), D	0.22
Scale ratio (λ)	3.41
Number of Blades, Z	5
P/D at 0.7R	0.8475
Expanded Blade Area Ratio	1.057
Hub to Propeller Diameter Ratio (D_H/D)	0.18
Rake Angle (°)	0
Skew Angle (°)	19
Propeller Type	Fixed Pitch
Blade Loading Distribution	NACA $a = 0.8$
Thickness Distribution	NACA 66 modified

Table 2. The details of the test condition.

Parameter	Symbol	Value
Inflow speed (m/s)	V_A	3.08
Propeller rotational rate (rps)	n	35
Advance ratio	J.	0.4
Cavitation number	σ_N	1.3

validated with the experimental data for this condition. The details of the test case are given in Table 2.

4. Computational domain design and grid structure

4.1. Computational domain design

A rectangular domain was used in the numerical calculations to replicate the measurement section of the cavitation tunnel. The cavitation and noise experiments were conducted at the Cavitation Tunnel of the University of Genoa. The tunnel has 0.57×0.57 m square test section, and the total length of the test section is around 2.2 m (Tani et al. 2017). Figure 3 provides an overview of the computational domain used in this study.

The positive X side of the computational domain is the velocity inlet, whereas the negative X side of the domain is defined as a pressure outlet in Figure 3. The computational domain dimensions were tuned to replicate the cavitation tunnel. The total length of the computational domain is defined as 2.2 m. The axial distance between the centre of the propeller blades and the inlet of the computational domain was set to 2.5D, whereas the axial distance between the centre of the propeller blades and outlet of the computational domain was set to approximately 7.5D. The width and height of the computational domain are identified as 0.57 m. The diameter and length of the rotating region were set to 1.13D and 1.05D, respectively. The three different regions (i.e. static, rotating and noise surface) were created in the computational domain for two complementary purposes. The rotating region was utilised to describe the propeller rotational motion, while the porous noise region was utilised for the URN prediction. The propeller blades and shaft were identified as a wall with the no-slip condition to satisfy the kinematic boundary conditions. Additionally, the no-slip condition was also identified on the tunnel walls.

4.2. Grid structure

The application of the suitable grid structure is one of the key solution parameters in the numerical calculations. Unsuitable grid structures cause an excessive amount of discretisation errors in the numerical solvers. From the viewpoint of the hydrodynamic performance prediction of a propeller (i.e. thrust and torque), the solution is less dependent on the grid structure; thus, the good agreement between the CFD and experiment can be even obtained using relatively coarse grids under non-cavitating conditions. However, when the propeller's wake and cavitation are of great interest, it requires special attention to model such complex flow around the propeller blades, especially in the tip region of the blades for the accurate definition of the TVC. Therefore, apart from the numerical scheme and turbulence modelling, a suitable grid should be adopted for the realistic solution of the cavitation dynamics. As well as the overall grid structure, the observation of TVC is strongly depended on the adequate mesh size inside the vortex core (Gaggero et al. 2014; Asnaghi et al. 2020). In order to adopt sufficient grid structure for the observation of

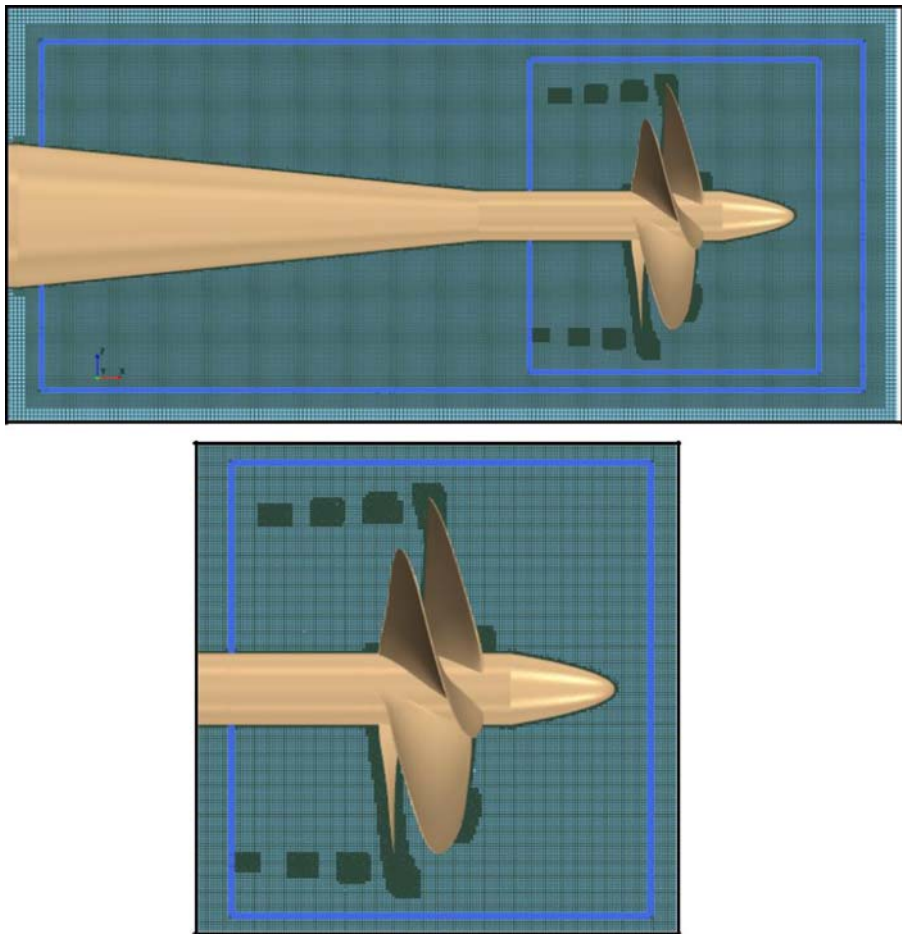

Figure 4. General view of the grid structure around the propeller blades. (This figure is available in colour online.)

TVC, the special mesh techniques (e.g. AMR) can be employed locally to decrease the computational cost of the solutions.

From the hydroacoustic perspective, the numerical or non-physical noise issue is one of the crucial problems in the numerical solvers. This is mainly triggered by the sliding interfaces in the sliding mesh technique; hence, it is important to perform uniform cell size in the computational domain without any mesh transitions, particularly in the noise region. In this way, the numerical noise can be decreased considerably (Star CCM 14.06+ 2019).

By considering both hydrodynamic and hydroacoustic perspectives, the unstructured grid with hexahedral elements was adopted to discretise the computational domain in the facilities of Star CCM+ (Star CCM 14.06+ 2019). Trimmer mesh was used with minimal skewness cells by the combination of the AMR technique. AMR is a dynamic method that refines or coarsens the cells in the specified regions of the domain based on the adaptive mesh criteria. Due to the difficulties of the determination for the refinement criteria, the AMR procedure is not easy to conduct for complex problems. In the cavitating propeller applications, the refinement criteria of the AMR can be selected either pressure or vorticity for the observation of TVC. As the pressure is a scalar quantity and pressure field looks similar to a Gaussian function in the transversal direction of the tip vortex, which is clearly stated in the study of Yvin and Muller (2016), it is hard to determine whether the minimum pressure is located in the centre of the tip vortex or not. As stated in the study of Yvin and Muller (2016), the refinement criteria should not be based on the pressure itself. Therefore, in this study, the gradient quantity (i.e. vorticity) was used as a refinement criterion for the AMR technique. The vorticity-based AMR approach was implemented in the rotating region using the developed user-based field functions. For the determination of the cell size inside the vortex core, Asnaghi (2018) and Asnaghi et al. (2020) conducted a comprehensive numerical study for the determination of required cell size for the accurate tip vortex solution for an elliptical foil. In addition to these studies, other comprehensive experimental tests were conducted by Kuiper (1981), using different model scale propellers for the investigations of the bubble, sheet, and tip vortex cavitation. In Kuiper's dissertation, the relationship between cavitation

Table 4. Comparison and validation of the numerical results with the experiment.

Viable	CFD (RANS)	CFD (DES)	Experiment (EFD)
K_T.	0.261	0.262	0.244
$10K_Q$.	0.365	0.365	0.341
η_0.	0.455	0.456	0.455

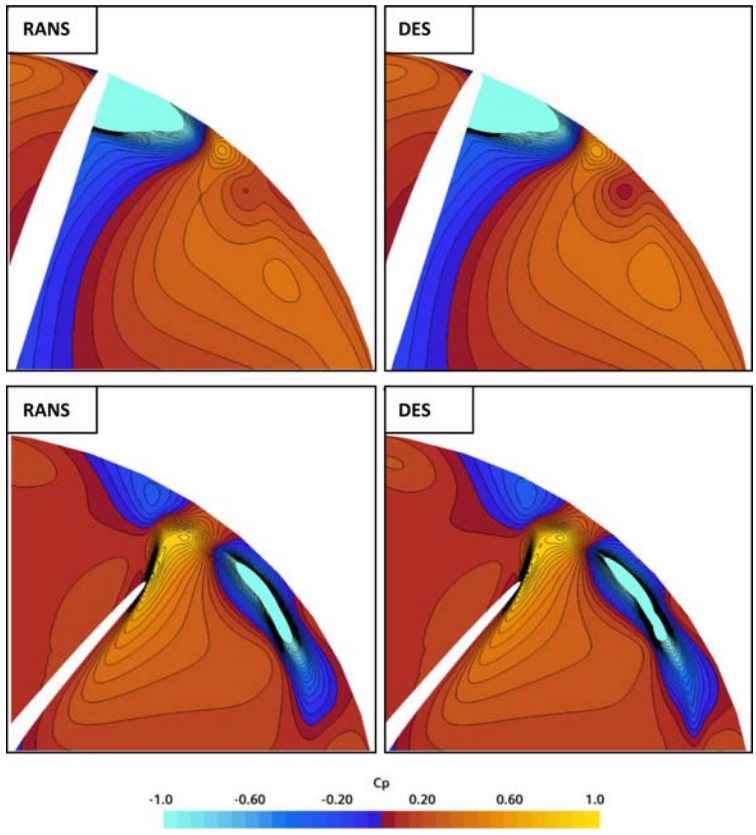

Figure 5. Comparison of non-dimensional pressure coefficient (above: $x/D = 0.05$; below: $x/D = 0.1$). ($C_p = (P/0.5\rho(nD)^2)$). (This figure is available in colour online.)

index (σ) and core radius (a_c) was explored. According to experimental results, the core radius at the inception was measured around 0.25 mm at model scale. In this study, by taking recommendations of the comprehensive studies above, cell size in the vortex core was set to 0.2 mm for observation of TVC. The proposed V-AMR approach consists of two stages, namely the 1st and the 2nd stages. When the flow field converges, the trajectory of the tip vortex is visualised using the threshold value of the vorticity based Q-criterion. Following this, the tip vortex trajectory is created by applying the relatively coarse grids at the 1st stage of the V-AMR. After a few propeller rotations, the 2nd stage of the V-AMR is implemented with 0.2 mm grid size using the new-threshold value of the Q criterion for the observation of TVC in the propeller's slipstream. The reason being, two stages V-AMR technique make the solution more computationally affordable as it prevents the generation of redundant cells outside of the tip vortex region, which is not of great interest. It is also noted that the redundant cells around the propeller hub were prevented using an additional user-based field function before the V-AMR procedure was implemented. The total element count can increase, typically, from around 20 M to 29 M using the V-AMR method for modelling all propeller blades when the longest noise region is used. It is to be noted that the proposed V-AMR technique can also be applied for the accurate solution of the hub vortex and hence the hub vortex cavitation. However, as the propeller operates in pulling configuration in this study, the hub vortex cavitation is not of great interest.

The general view of the grid structure with AMR can be seen in Figure 4. It should be noted that in the presence of the AMR, the CFL number increases in the vortex cores. To keep the CFL number around 1 inside the vortex, the time step should be reduced significantly (e.g. around 0.2 degrees), but this increases the computational cost of the solution. The extension of the TVC in the propeller's slipstream does not create considerable changes if the timestep is selected between 1 and 0.5 degrees of propeller's rotational rate. Similar comments for the extension of TVC with different timesteps can also be found in the study of Krasilnikov (2019).

5. Numerical results

5.1. Hydrodynamic results

The numerical results obtained by the RANS and DES solvers are validated with the experimental data from the University of Genoa Cavitation Tunnel (UNIGE), as shown in Table 4. The difference between CFD and EFD was found around 7% for thrust and torque values. The RANS and DES solvers showed similar results for the prediction of hydrodynamic characteristics.

The further analysis between RANS and DES solvers were conducted in the propeller's slipstream with the axial planes located in the propeller's slipstream at $x/D = 0.05$–0.1, and 0.2. As shown in Figure 5, the non-dimensional pressure contours show a similar trend, except at the cavitating tip vortex regions. The AMR technique enables to capture further reduced pressures in the vortex regions for the observation

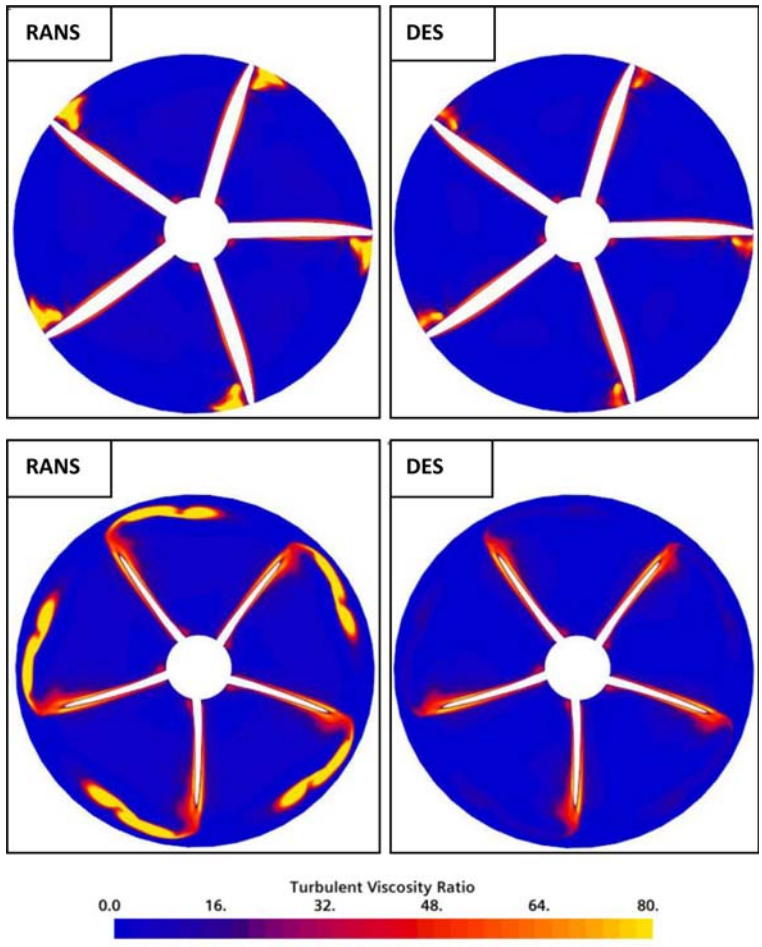

Figure 6. Comparison of eddy viscosity ratio (μ_t/μ) (Above: $x/D = 0.05$; Below: $x/D = 0.1$). (This figure is available in colour online.)

of TVC. The low-pressure part is found to be more extended in the DES solver at the propeller blade tips where TVC first occurs.

Figure 6 shows the turbulent eddy viscosity ratio (also known as the eddy viscosity ratio), which is the ratio of the turbulent viscosity (μ_t) and dynamic molecular viscosity (μ), calculated by the RANS and DES solvers. Eddy viscosity ratio can also be considered as an indication of the additional dissipation created by the turbulence model. As shown in Figure 6, the RANS method produces an excessive amount of eddy viscosity when compared to DES solver at the propeller blades tips. Thus, the generation of higher eddy viscosity in the RANS solver may cause an inadequate solution of cavitation dynamics in unsteady cavitation simulations (Li et al. 2014; Lloyd et al. 2017).

Due to the lack of experimental flow data in the propeller's slipstream, the axial velocity distributions calculated by the RANS and DES solvers are compared with each other at $x/D = 0.2$ in Figure 7. As shown in this figure, DES solver presents a definitive pattern for the strength and details of the flow field at the propeller blade tip in comparison to the prediction of the RANS method. Consequently, the RANS method failed to predict the vortex core velocities as accurate as of the DES solver.

As well as the comparison of flow details in the propeller's slipstream, the sheet and tip vortex cavitation pattern, which were predicted by the RANS and DES solvers, were compared with the experimental observation in Figure 8. The sheet cavitation pattern on the propeller blades was predicted similarly using both the RANS and DES solvers. Moreover, the results are found in a good agreement with the experiment, as shown in Figure 8. The results also indicate that the RANS solver can be reliably used for the prediction of the sheet cavitation on the blades. Nevertheless, the inherent modelling errors of the RANS solver might cause an inadequate solution of important cavitation dynamics, and it needs to be further investigated in a study solely focused on this subject.

As it is known, the RANS solvers mainly suffer from both the discretisation and modelling errors, which result in numerical diffusion in the numerical solutions (Feder and Abdel-Maksoud 2016). In particular, the excessive amount of turbulence intensity inside the vortex core is one of the deficiencies of the standard RANS solvers in terms of the accurate solution of the tip vortex flow (see Figure 6). It consequently leads to the failure in capturing the flow dynamics inside the vortex core when compared to scale resolving simulations (i.e. DES and LES). As it is observed in Figure 6, the higher eddy viscosity predicted inside the vortex with the RANS solver causes an inadequate extension of the TVC in comparison to that of the TVC from the DES solver, which can be clearly seen in Figure 8. In the meantime, the formation pattern and further extension of the TVC in the propeller's

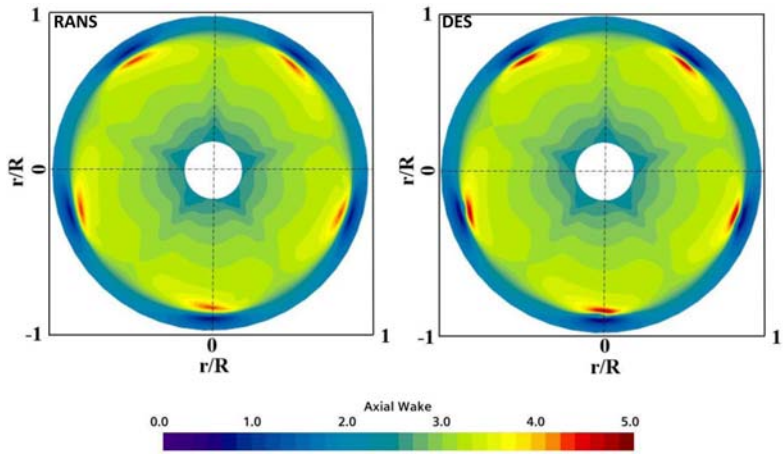

Figure 7. Comparison of axial wake ($V_A - V_X/V_A$) at $x/D = 0.2$. (This figure is available in colour online.)

slipstream are found to be promising with the DES solver in comparison to the experimental view that can also be seen in Figure 8.

5.2. Hydroacoustic results

The hydroacoustic performance of the benchmark propeller was investigated using the DES with P-FWH equation due to the several inherent modelling errors of the RANS solver, which were discussed in the previous section. The application of scale resolving simulations (i.e. DES or LES) with the acoustic analogy is a state-of-art method for the propeller URN studies. In this study, the porous surface (or integral surface, PS), indicated by the blue colour in Figure 9, was located around the propeller blades to include relevant non-linear noise contribution, which is mainly represented by the vorticity and turbulence in the propeller's slipstream. Furthermore, the two different porous surfaces were also used to show the convergence of the hydroacoustic predictions. The geometric properties of selected porous surfaces are given in Table 5. The hydroacoustic data was collected on the selected porous surfaces during the computations.

In order to show the reliability of the numerical solution, the hydroacoustic pressures can be compared with the hydrodynamic pressures in the near field (i.e. in the vicinity

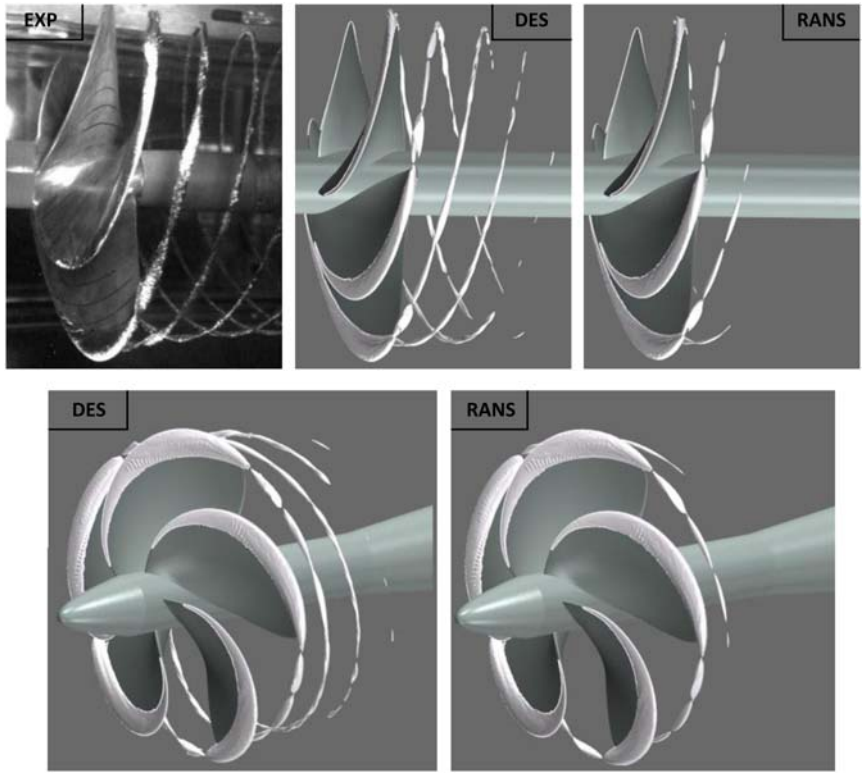

Figure 8. Comparison of sheet and tip vortex cavitation with the experimental observation (vapor volume fraction (α_v) = 0.1). (This figure is available in colour online.)

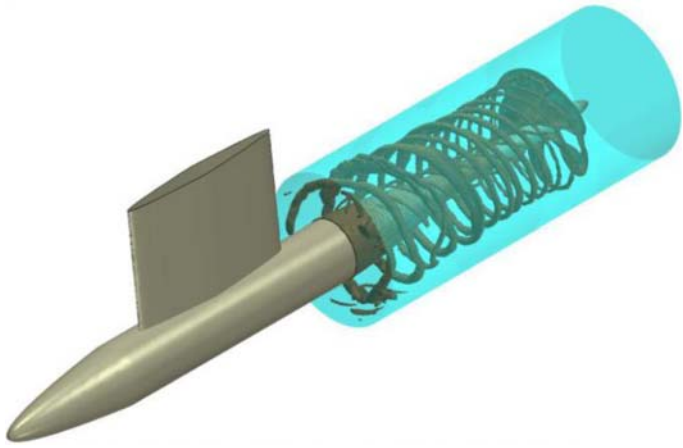

Figure 9. Visualisation of porous surface (PS1) and tip vortex trajectory ($Q = 40.000\ 1/sn^2$). (This figure is available in colour online.)

of the propeller). In this way, the consistency of the solution can be proved for far-field noise estimation. Figure 10 shows the comparison of the hydrodynamic and hydroacoustic pressures in the near field at the propeller plane. The pressures can be compared everywhere in the vicinity of the propeller. The comparison of two pressures shows that hydrodynamic pressure might be used instead of the acoustic pressure in the close proximity of the propeller. As far away from the noise source, the acoustic analogy is needed to employ for the prediction of the URN. The reason being that the hydrodynamic pressures tend to be affected by numerical diffusion in the numerical solvers. Furthermore, Figure 10 also shows the change in hydroacoustic pressures with different porous surfaces. As shown in Figure 10, the hydroacoustic pressures of the different porous surfaces are similar and superimpose each other. Thus, the convergence of the hydroacoustic solution can also be proven.

Following the verification of the acoustic analogy, the numerical results were compared with the experimental data. In the experiment, the acoustic pressures were measured at three different receivers. The experimental results were extrapolated to 1 m using the averaged spectra of three hydrophones and only taking the HP3 results with the help of the transfer functions. The locations of the receivers and coordinate system are given with respect to the centre of the propeller blades in Table 6 and Figure 11, respectively. The positive X direction is upstream of the propeller.

In the numerical calculations, the acoustic pressures were measured both at 1 m and each receiver locations. Following that, the results computed at HP3 and averaged spectra of the three hydrophones were extrapolated to 1 m using ITTC distance normalisation. Figures 12 and 13 show the comparison of the numerical results with the experimental data at 1 m using only HP3 receiver and averaged spectra of three receivers, respectively. As shown in Figures 12 and 13, the overall trend of the numerical result is in agreement with the experimental data.

In Figure 12, the numerical results underpredicted the noise levels around 10 dB in the low-frequency region until 1 kHz. In the mid-frequency range (i.e. between 1 and 2 kHz), the results are in a good agreement with the experimental data. Similar to the low-frequency range, the noise levels were underpredicted approximately 5–10 dB in the high-frequency content of the noise spectrum. The 1st BPF (Blade Passage Frequency) value at 175 Hz is more distinct in the noise spectrum, particularly for the extrapolated data, whereas 2nd, 3rd and other peaks are visible in the spectra with small amplitudes. The noise levels are also compared by taking the averaged spectra of three hydrophones in Figure 13. Unlike the numerical results at HP3, the discrepancy between the experiment and numerical solution reduces approximately 1–5 dB in the low-frequency range until 1 kHz. The 1st and 2nd BPF values were well predicted in the numerical calculations. Similar to HP3

Table 5. Geometrical properties of selected porous surfaces (L is the length of the PS, D_{PS} is the diameter of the PS).

PS ID	L/D	D_{PS}
1	3.0	1.26D
2	2.5	1.25D
3	2.0	1.24D

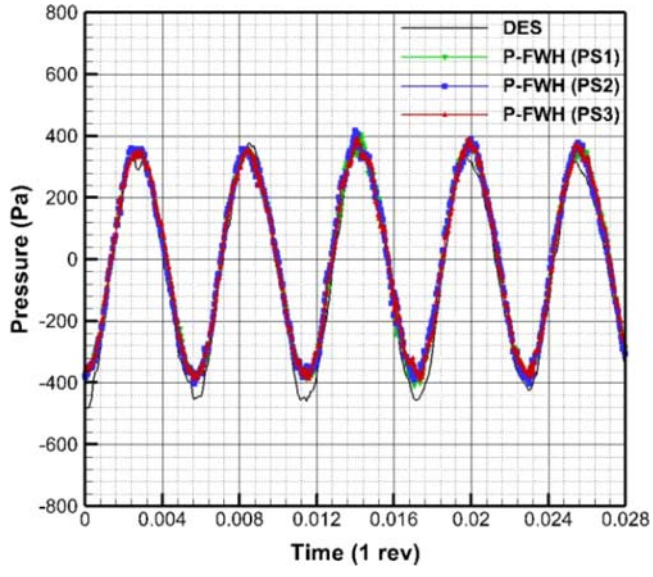

Figure 10. Comparison of hydrodynamic and hydroacoustic pressures at 0.17 m from the centre of propeller blades at the propeller plane. (This figure is available in colour online.)

Table 6. Locations of the receivers.

–	Coordinates (mm)		
Hydrophones	*X*	*Y*	*Z*
HP1	−54.5	0	−393
HP2	−49.5	163	0
HP3	−125.5	−142	−120

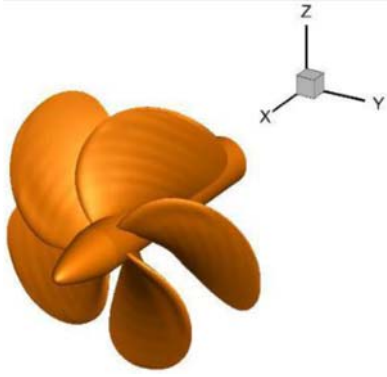

Figure 11. The coordinate system around the propeller blades. (This figure is available in colour online.)

results, the noise levels are slightly underpredicted in the high-frequency region of the noise spectrum in the numerical calculations in comparison with the experiment. In the measurement, there is a distinct peak at around 740 Hz, which is not present in the numerical prediction. This peak is also present in the background noise measurements. This peak occurs due to the mechanical vibration of one of the two hydrophone supports. Thus, it is evaluated as a background noise component. It is expected to be removed by the background noise correction. However, the intensity of this noise component is higher when the propeller is present in the tunnel section since the propeller induced pressure pulses may contribute further to the structural vibration of these supports. Due to this fact, this noise component is not relevant for the comparison of numerical results with the experimental data. The detailed discussion about this peak can be found in (Tani et al. 2017).

Figures 12 and 13 also shows the noise levels computed directly at 1 m. As can be seen in Figures 12 and 13, the differences between the two different numerical results (i.e. extrapolated and direct calculation) originate from the ITTC distance formulation. Also, the numerical results obtained by different porous surfaces in P-FWH equation is also compared in Figures 12 and 13. As shown in Figures 12 and 13, even though the overall trend of the noise spectrum is similar in three different porous surfaces, there are some slight differences at the peak values computed by different porous surfaces. In particular, some BPF values are more distinct using the PS3. Although all porous surfaces are located inside the fine grid region to minimise the information loss due to the discretisation errors, the relatively smaller porous surface (i.e. PS3), which covers the most energetic vortical structures of turbulence, seems to capture more detailed information in the

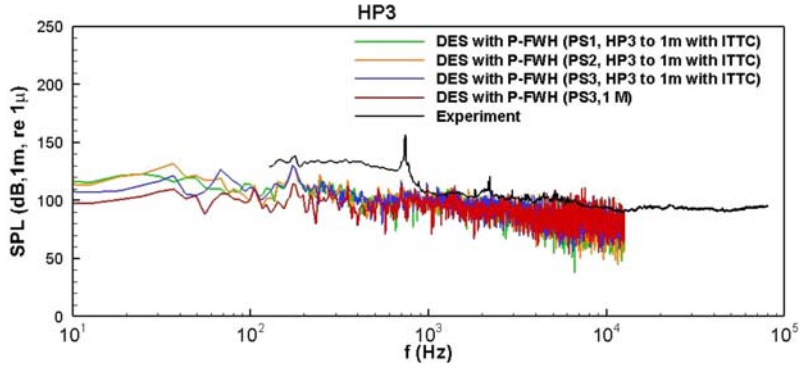

Figure 12. Comparison of numerical results and experimental data in narrowband at 1 m using HP3 receiver. (This figure is available in colour online.)

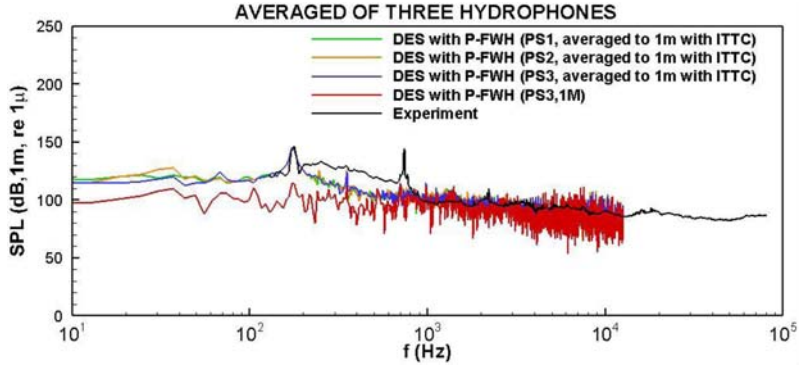

Figure 13. Comparison of numerical results and experimental data in narrowband at 1 m using averaged data of three hydrophones. (This figure is available in colour online.)

noise spectrum. However, as stated in the several studies (e.g. Bensow and Liefvendahl 2016; Li et al. 2018), exact location and placement of the porous surface have still been discussed and have not been fully understood yet in the current literature. Therefore, selecting a suitable porous surface should also be investigated further with an in-depth study, particularly under non-uniform flow conditions and far-field. The noisy signal can also be seen in the high-frequency part of the noise spectrum. This may be because of the short sampling time, which was six revolutions in the numerical calculation. Although time sampling frequency is 25.2 kHz, as stated in the study of Bensow and Liefvendahl (2016), the short sampling time may trigger the noisiness of the signal.

6. Conclusions

The present study showed the capabilities of DES and RANS solvers for the solution of the flow around the cavitating propeller in a comparative manner. In numerical simulations, the Schnerr-Sauer cavitation model, which was coupled with the proposed vorticity-based AMR technique, was utilised for both solvers. The RANS and DES solvers were compared each other in terms of propeller performance characteristics, sheet cavity patterns on the propeller blade, and TVC extensions in the propeller's slipstream. Additionally, the detailed analysis was also conducted at the planes located in the propeller's slipstream using the RANS and DES solvers. The cavitation pattern, thrust and torque coefficients were validated with the experimental data. Based on this investigation, it was found that:

- The sheet cavity pattern on the propeller blades was predicted similarly using both RANS and DES solvers. However, the flow details (e.g. pressure, turbulent eddy viscosity, velocity) was predicted dissimilar and thus the TVC. The results showed that the RANS method produces an excessive amount of eddy viscosity at the propeller blade tips where TVC first occurs. Since the higher eddy viscosity increases the numerical diffusion in the calculations, the RANS method fails to capture the TVC as accurate as of the DES solver. In contrast, the DES method showed promising results for the extension of TVC in comparison with the experimental observation. In addition, the flow details in DES solver were predicted better than RANS solver at the propeller blade tips.

Finally, the hydroacoustic performance of the propeller was predicted by combining the DES solver with the P-FWH equation. In this regard, hydrodynamic and hydroacoustic pressures were compared with each other in the near field. Thus, the consistency of the numerical solution was proved. Three different integral surfaces were utilised to show the convergence of the hydroacoustic solution. Following that, the numerical prediction of the propeller URN results was compared with the experimental data. Based on this investigation, it was found that:

- The overall trends of the noise spectrum for HP3 and averaged data of three hydrophones in the numerical calculations were found in a good agreement with the experimental data. The discrepancies were observed both in low and high-frequency ranges. It is important to note that the computational domain was modelled to replicate the cavitation tunnel in the scope of this study. However, the results will also be compared at 1 m by modelling the free-field conditions in the further studies as the transfer function is mainly used to transfer the data from the confinement region to free-field condition in the cavitation tunnels.

The work presented in this paper is an ongoing research study to predict the propeller URN in full-scale as well as exploring further aspects of real physics of the full-scale flow. Within this framework, this study is currently being extended to include the effects of hull flow and roughness on the propeller URN.

Acknowledgements

The first author is sponsored by Stone Marine Propulsion Ltd of the UK and the University of Strathclyde during his PhD study. Results were obtained using the ARCHIE-WeSt High-Performance Computer (www.archie-west.ac.uk) based at the University of Strathclyde. The authors also thank Dr Giorgio Tani for providing the experimental results.

Disclosure statement

No potential conflict of interest was reported by the author(s).

ORCID

Savas Sezen http://orcid.org/0000-0002-0852-0145

References

AMT'11. 2011. 2nd International Conference on Advanced Model Measurement Technology for the EU Maritime Industry, AMT'11, Newcastle University, Newcastle Upon Tyne, April.

AQUO. Achieve Quiter Oceans by shipping noise footprint reduction. 7th framework program, Grant Agreement No: 314227.

Asnaghi A. 2018. Computational modelling for cavitation and tip vortex flows [PhD thesis]. Goteborg, Sweden: Department of Mechanics and Maritime Sciences, Chalmers University of Technology.

Asnaghi A, Svennberg U, Bensow R. 2020. Large eddy simulation of cavitating tip vortex flows. Ocean Eng. 195:106703.

Atlar M, Aktas B, Sampson R, Seo K-C, Ignazio MV, Fitzsimmons P, Fetherstonhaug C. 2013. A multi-purpose marine science & technology research vessel for full-scale observations and measurements. Proceedings of the 3rd International Conference on Advanced Model Measurement Technologies for the Maritime Industry, AMT'13; September; Gdansk.

Bal S. 2011. A method for optimum cavitating ship propellers. Turk J Eng Environ Sci. 35(3):139–158.

Bensow RE, Bark G. 2010. Implicit LES predictions of the cavitating flow on a propeller. J Fluids Eng. 132(4):041302.

Bensow RE, Liefvendahl M. 2016. An acoustic analogy and scale-resolving flow simulation methodology for the prediction of propeller radiated noise. 31st Symposium on Naval Hydrodynamics; Sept 11–16; Monterey, CA.

Di Francescantonio P. 1997. A new boundary integral formulation for the prediction of sound radiation. J Sound Vib. 202(4):491–509.

Feder D-F, Abdel-Maksoud M. 2016. Tracking a tip vortex with adaptive vorticity confinement and hybrid RANS-LES. Open J Fluid Dyn. 6:406–429.
Gaggero S, Tani G, Viviani M, Conti F. 2014. A study on the numerical prediction of propellers cavitating tip vortex. *Ocean Eng* 92:137–161.
Guilmineau E, Deng GB, Leroyer A, Queutey P, Visonneau M, Wackers J. 2015. Influence of the turbulence closures for the wake prediction of a marine propeller. Fourth International Symposium on Marine Propulsors, smp'15; Austin, TX, USA.
Hildebrand JA. 2009. Anthropogenic and natural sources of ambient noise in the ocean. Mar Ecol Prog Ser. *395*:5–20.
Ianniello S, Muscari R, Di Mascio A. 2013a. Ship underwater noise assessment by the acoustic analogy. Part I: non-linear analysis of a marine propeller in a uniform flow. J Mar Sci Technol. 18:547–570.
IMO. 2014. Guidelines for the reduction of underwater noise from commercial shipping to address adverse impacts on marine life. MEPC.1/Circ.833.
ITTC. 2011. Recommended procedures and guidelines (7.5-03-01-04). CFD, general CFD verification.
ITTC. 2017. Specialist committee on hydrodynamic noise, 28th ITTC, volume III.
Kellett P, Turan O, Incecik A. 2013. A study of numerical ship underwater noise prediction. Ocean Eng. 66:113–120.
Kinnas S, Fine N. 1992. A non-linear boundary element method for the analysis of unsteady propeller sheet cavitation. Proceedings of the 19th Symposium on Naval Hydrodynamics, p. 717–737; Seoul, Korea: National Academy Press.
Krasilnikov V. 2019. CFD modelling of hydroacoustic performance of marine propellers: Predicting propeller cavitation. Numerical Towing Tank Symposium (NuTTS), Portugal.
Kuiper G. 1981. Cavitation Inception on Ship Ship Propeller Models. PhD Thesis, Delft University of Technonology, Delft, Netherlands.
Li D-Q, Hallander J, Johansson T. 2018. Predicting underwater radiated noise of a full-scale ship with model testing and numerical methods. Ocean Eng. 161:121–135.
Li Z, Pourquie M, van Terwisga T. 2014. Assessment of cavitation erosion with a URANS method. J Fluids Eng. 136(4):041101.
Lidtke A, Lloyd T, Vaz G. 2019. Acoustic modelling of a propeller subject to non-uniform inflow. Sixth International Symposium on Marine Propulsors, SMP2019, Rome, Italy.
Lighthill MJ. 1952. On sound generated aerodynamically I. General theory. Proc R Soc London A. 211:564–587.
LLoyd TP, Rijpkema D, van Wijngaarden E. 2015. Marine propeller acoustic modelling: comparing CFD results with an acoustic analogy method. Fourth International Symposium on Marine Propulsors Smp'15. Austin, TX.
Lloyd TP, Vaz G, Rijpkema D, Reverberi A. 2017. Computational fluid dynamic prediction of marine propeller cavitation including solution verification. Fifth International Symposium on Marine Propulsors Smp'17, Espoo; June 2017.
Muscari R, Di Mascio A, Verzicco R. 2013. Modeling of vortex dynamics in the wake of a marine propeller. Comput Fluids. 73:65–79.
Peng HH, Qiu W, Ni S. 2013. Effect of turbulence models on RANS computation of propeller vortex flow. Ocean Eng. 72(1):304–317.
Salvatore F, Streckwall H, Terwisga T. 2009. Propeller cavitation modelling by CFD results from the VIRTUE 2008 Rome workshop. First International Symposium on Marine Propulsors Smp09; Trondheim, Norway.
Schnerr GH, Sauer J. 2001. Physical and numerical modelling of unsteady cavitation dynamics. Int Conf Multiphase Flow. 11:391–400.
Sezen S, Atlar M, Fitzsimmons P, Sasaki N, Tani G, Yilmaz N, Aktas B. 2019. Numerical cavitation noise prediction of a benchmark research vessel propeller, The Sixth International Conference on Advanced Model Measurement Technology for The Maritime Industry, AMT'19; Rome, Italy.
Sezen S, Atlar M, Fitzsimmons P, Sasaki N, Tani G, Yilmaz N, Aktas B. 2020. Numerical cavitation noise prediction of a benchmark research vessel propeller. Ocean Eng. 211:107549.
Sezen S, Kinaci OK. 2019. Incompressible flow assumption in hydroacoustic predictions of marine propellers. Ocean Eng. 186:106138.
SILENV. Ships oriented innovative solutions to reduce noise and vibrations. 7th framework program, Grant Agreement No: 234182.
Sipilä T. 2012. RANS analyses of cavitating propeller flows, PhD Thesis, Espoo, Finland: School of Engineering, Aalto University.
Sipilä T, Sanchez CA, Siikonen T. 2014. Eddy vorticity in cavitating tip vortices modelled by different turbulence models using the RANS approach. 6th European Conference on Computational Fluid Dynamics (ECFD VI); Barcelona, Spain.
SMP11. 2011. Workshop on cavitation and propeller performance.
SONIC. Suppression of underwater noise induced by cavitation. EC-FP7, Grant Agreement No: 2012 314394.
Spalart PR, Deck S, Shur ML, Squires KD, Strelets MK, Travin A. 2006. A new version of detached-eddy simulation, resistant to ambiguous grid densities. Theo Comput Fluid Dyn. 20:181.
Star CCM. 2019. Siemens, Star CCM 14.06, user guide.
Tani G, Aktas B, Viviani M, Atlar M. 2017. Two medium size cavitation tunnel hydroacoustic benchmark experiment comparisons as part of a round robin test campaign. Ocean Eng. 138:179–207.
Tani G, Aktas B, Viviani M, Yilmaz N, Miglianti F, Ferrando M, Atlar M. 2019a. Cavitation tunnel tests for "The Princess Royal" model propeller behind a 2-dimensional wake screen. Ocean Eng. 117:829–843.
Tani G, Viviani M, Felli M, Lafeber F, Lloyd T, Aktas B, Atlar M, Seol H, Hallander J, Sakamoto N, Kamiirisa N. 2019b. Round Robin test on radiated noise of a cavitating propeller. Sixth International Symposium on Marine Propulsors, SMP2019; Rome, Italy.
Testa C, Porcacchia F, Greco L, Muscari R. 2018. Effectiveness of boundary element method hydrodynamic data for propeller hydroacoustics. A. Yucel Odabasi Colloquium Series 3rd International Meeting-Progress in Propeller Cavitation and Its Consequences: Experimental and Computational Methods for Predictions; Istanbul, Turkey, p. 77–85.
Urick RJ.. 1983. Principles of Underwater Sound, 3rd Edition. Peninsula Publishing. ISBN 0932146627.
Usta O, Korkut E. 2018. A study for cavitating flow analysis using DES model. Ocean Eng. 160:397–411.
Viitanen VM, Siikonen T. 2017. Numerical Simulation of Cavitating Marine Propeller Flows. 9th International Conference on Computational Mechanics MekIT'17; Trondheim, Norway.
Wilcox DC. 2006. Turbulence modeling for CFD. In: Industries, D.C.W., Canada, La, Calif (Eds.), 3rd ed.
Williams JEF, Hawkings DL. 1969. Sound generation by turbulence and surfaces in arbitrary motion. Phil Trans R Soc London A. 264:321–342.
Yvin, C., Muller, P. 2016. Tip Vortex Cavitation Inception without a cavitation model. 19th Numerical Towing Tank Symposium; France.